Computation of Periodic Orbits for Piecewise Linear Oscillator by Harmonic Balance Methods

Lijun Pei[a,b], Antonio S.E. Chong[b], Ekaterina Pavlovskaia[b], Marian Wiercigroch[b*]

[a] *School of Mathematics and Statistics, Zhengzhou University, Zhengzhou, Henan, 450001 China*
[b] *Centre for Applied Dynamics Research, School of Engineering, University of Aberdeen, Aberdeen, AB24 3UE Scotland, UK*

Abstract

In this paper, Harmonic Balance based methods, namely Incremental Harmonic Balance Method and the method of Harmonic Balance with Alternating Frequency and Time traditionally used to compute periodic orbits of smooth nonlinear dynamical systems are employed to investigate dynamics of a non-smooth system, a piecewise linear oscillator with a play. The Incremental Harmonic Balance Method was used to compute the period one orbits including those exhibiting grazing and large impacts. The method of Harmonic Balance with Alternating Frequency and Time was implemented to calculate more complex orbits and multi stability. A good agreement between obtained approximate solutions and numerically calculated responses indicates robustness of the implemented HBMs, which should allow to effectively study the global dynamics of non-smooth systems.

Keywords: Piecewise linear oscillator with play, Incremental Harmonic Balance Method, IHBM, Harmonic Balance with Alternative Frequency and Time, HB-AFT, Computation of periodic orbits

1. Introduction

Mathematical models of non-smooth systems have been extensively studied in the past decades by both analytical and numerical methods. The periodically forced single degree-of-freedom piecewise linear oscillator is the archetype of such systems, where the non-smoothness is present in the restoring force, which was first comprehensively investigated by Shaw and Holmes [1]. Another type of a single degree-of-freedom piecewise linear oscillator namely oscillator with a backlash or a play considered in this paper was studied earlier by Kleczka *et al.* [2]. Luo *et al.* [3] numerically investigated its global chaotic behaviour and Wiercigroch [4] provided a further overview of the system dynamics through computing codimension-1 bifurcation diagrams. In addition, it is relevant

*Corresponding author. Email: m.wiercigroch@abdn.ac.uk (M. Wiercigroch). Tel.: +44(0) 1224 272509; Fax: +44(0) 1224 272497.

to mention the works on gear systems with a backlash by Kaharaman *et al.* [5], Theodossiades *et al.* [6] and de Souza *et al.* [7]. An exact solution for periodic symmetric responses in an oscillator with a symmetrical trilinear spring subjected to harmonic excitation was considered by Natsiavas [8] and reflected upon by contrasting again other non-smooth systems in his recent compressive review [9].

To analyse the motion undergoing grazing impacts, several methods were proposed. The discrete mapping and the discontinuity mapping were respectively developed and employed to investigate the dynamics of the grazing cases by Nordmark [10] and Dankowicz and Nordmark [11]. Then the latter was generalized to the system with discontinuities in the vector field by Molenaar *et al.* [12] and Dankowicz and Zhao [13]. The other unique behaviour of piecewise smooth systems is the so-called border–collision bifurcation, and classification of border–collision bifurcation scenarios can be found in works by di Bernardo *et al.* [14]. Nusse and Yorke [15] provided a general criterion for the occurrence of such bifurcations in two-dimensional piecewise smooth maps. Moreover, their classification was also discussed by Banerjee and Grebogi in [16].

Di Bernardo *et al.* [17], [18] presented a unified framework for grazing and sliding bifurcations in n-dimensional piecewise smooth dynamical systems of ODE's by deriving their normal form Poincaré maps. Impacting systems between rigid and elastic impact oscillators have been studied by Ma *et al.* [19]. Furthermore, in [20] the effects of the individual components on the character of the normal form map were numerically and experimentally investigated.

Among other important experimental investigations concerned with grazing events are those conducted by Stensson *et al.* [21], by Piiroinen *et al.* [22] and by the Centre of Applied Dynamics Research at the University of Aberdeen [23] – [27]. In [25], a narrow band of chaos near the grazing condition was discovered and in [26], a rich dynamical behaviour of the oscillator close to grazing was unveiled by analysing bifurcation scenarios with a large number of co-existing attractors. The study undertaken in [27] was focussed on the dynamics of the system with a play showing new types of bifurcations and providing for the first time a global overview of dynamics where all control system parameters except the gap were used. It also touched upon grazing and crisis bifurcations employing newly developed in-house Matlab-based computational suite ABESPOL [28, 29]. Various computational approaches have been applied recently to non-smooth dynamical systems including hybrid symbolic-numeric computations [30], a combined method of harmonic balance and path following [31] and a smoothing procedure to enable the use of the harmonic balance method effectively [32].

It is widely known that the piecewise linear systems may exhibit very rich dynamical behaviour [1, 33, 34]. However, it is difficult in general to obtain closed–form solutions even for

simplest nonlinear systems of these types. It is also difficult to analyze the piecewise linear systems employing the standard perturbation methods such as Poincaré–Lindstedt, multiple scale, or Krylov–Bogoliubov–Mitropolski methods [35, 36], since they are valid only for continuous and weakly nonlinear dynamical systems. However, Harmonic Balance Methods (HBM) based on the Galerkin approximation can deal with systems with strong nonlinearities as they do not require systems to be continuous. They have been originally developed to study structural vibration of elastic systems [37]. As explained in [38], the Incremental Harmonic Balance Method (IHBM) is particularly suitable for computer implementation. In this method, firstly, a periodic solution of nonlinear dynamical system is represented by a Fourier series with small number of harmonics and then the considered system is transformed into a set of linearized incremental algebraic equations in terms of the Fourier coefficients. Next, these linearized equations are solved iteratively in each incremental step, with the formulation being carried out when changing the number of harmonic terms in the Fourier series of the solutions. Finally, the Fourier coefficients can be determined if the obtained solution converges. Compared with the classical approaches, the IHBM is remarkably effective for obtaining solutions with a desired accuracy over a wide range of varying parameter, where both stable and unstable solutions being computed directly. The IHBM has already been successfully applied to a wide range of dynamical systems, for example [38] – [41]. IHBM can also be employed to investigate the bifurcation and route-to-chaos [42], analyze the nonlinear dynamics of the time-varying dynamical system [43], predict the limit cycle oscillations under uncertainty [44] and other nonlinear problems [45] – [48], where periodicity of the anticipated solutions is expected. The IHBM also finds its way in some class of piecewise linear dynamical systems, (see [49] –[52]). With regards to the system with play, although we have found in our recent study [27] a complex and rich dynamical behaviour numerically, the profound mathematical reason behind this work is to investigate periodic orbits in more rigorous manner. To this end, based on the work presented in [51, 52], we will model and analyse nonlinear vibration of the piecewise linear oscillator with a play [2, 27] by the IHBM.

The layout of this paper is as follows. Section 2 presents the mathematical model of the considered system and its global dynamics. In Section 3, the HB based methods are described. In Section 4, a numerical simulation is carried out to compare results obtained from direct numerical simulation and HB based methods. Finally, conclusions are drawn in Section 5.

2. Mathematical model of a system with play and its global dynamics

The physical model of the considered system is a single-degree-of-freedom oscillator excited by a harmonic external force. In this oscillator, the mass is attached to a linear damper and comes

into contact with a linear spring when the amplitude of the oscillations exceeds a gap.

The motion of the system is governed by the piecewise linear ordinary differential equation [4, 27, 28] which can be written in non-dimensional form as

$$x'' + 2\,\xi\,x' + g(x) = a\,\cos(\omega\tau)\,. \tag{1}$$

Here non-dimensional displacement x and time τ are defined by using a reference displacement and linear natural frequency. Prime stands for differentiation with respect to the non-dimensional time τ, a and ω are the non-dimensional forcing amplitude and frequency, ξ is the damping ratio and $g(x)$ is the non-dimensional restoring force given by

$$g(x) = \begin{cases} x - e & , \quad x > e \\ 0 & , \quad |x| \leq e \\ x + e & , \quad x < -e \end{cases} \tag{2}$$

where e is the non-dimensional gap.

The respective vector field of the system in non-autonomous and autonomous form is presented below in equations (3) and (4) respectively. In the autonomous form, $s = \omega\tau \mod 2\pi$ defines an angular variable.

$$\begin{cases} x' &= v \\ v' &= a\,\cos(\omega\tau) - 2\,\xi\,v - g\,(x) \end{cases}\,, \tag{3}$$

$$\begin{cases} x' &= v \\ v' &= a\,\cos(s) - 2\,\xi\,v - g\,(x) \\ s' &= \omega \end{cases}\,. \tag{4}$$

Direct numerical simulations for the considered system were presented in [27]. Those simulations were performed by using the computational suite of numerical codes for non-smooth systems, ABESPOL [28]. This suite enables the user to explore the dynamics of piecewise smooth dynamical systems by computing their responses through its module of direct numerical simulation and module of numerical continuation. Unlike any other available software, ABESPOL has these two modules connected, providing the user with the choice to start a numerical continuation directly from a bifurcation diagram computed by a direct numerical simulation. To run a numerical continuation, ABESPOL has an interface that connects it to the computational continuation core COCO [29], in a way that, the existing general-purpose routines supplied by COCO for continuation and bifurcation analysis of smooth and non-smooth dynamical systems are used in a user-friendly and quick manner.

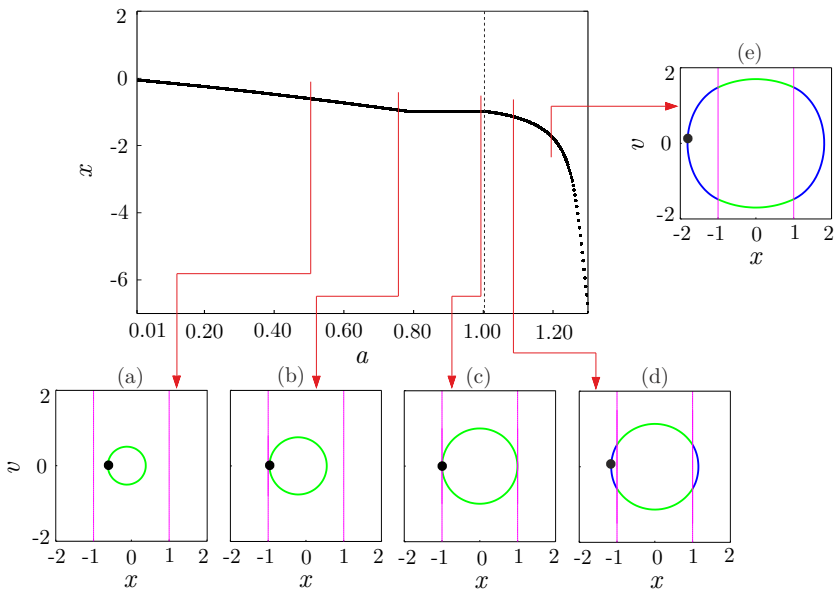

Figure 1: Bifurcation diagram of displacement as a function of the forcing amplitude, a, computed for $\xi = 0.02$, $e = 1$ and $\omega = 1$, where the control parameter was increased. Dashed vertical lines stand for grazing incidence. Additional panels show trajectories and Poincaré maps on the (x, v) planes computed for the following amplitudes: (a) $a = 0.50278$, (b) $a = 0.75820$, (c) $a = 0.99814$, (d) $a = 1.08330$, (e) $a = 1.19940$. There, operation in *No-Contact* mode is in green, whereas operation in *Contact-Up* and *Contact-Down* is in blue; points of the Poincaré maps are in the same colours used in the bifurcation diagram; and magenta vertical lines denote the discontinuity boundaries. Adopted from [27].

One of the bifurcation diagram computed by a direct numerical simulation in [27] is shown in Fig. 1, where the forcing amplitude was varied from 0.01 to 1.30. The other parameter values were fixed to ω =1.0, $\xi = 0.02$ and $e = 1.0$. As described in [27], each periodic orbit presents a number of crossings to the *Contact-Down* and to the *Contact-Up* modes. Because of this, they were classified as a period-(n, m, k) response, where n stands for its number of periods, and m and k stand for the number of crossings from the *No-Contact* mode to the *Contact-Down* mode and to the *Contact-Up* mode, respectively. The term symmetric was used for those responses whose trajectory has rotational symmetry with respect to the origin of coordinates of the (x, v) plane, and the term asymmetric was used otherwise.

In Fig. 1, with the increase of the forcing amplitude, non-impacting period-(1,0,0) attractors are observed at $a \in (0.0100\ ,\ 1.0007)$. Representative trajectories and Poincaré maps are shown in Figs 1(a) – 1(c). A grazing incidence, at $a = 1.00330$, takes place giving birth to period-(1,1,1) attractors, for which representative examples are shown in Figs 1(d) and 1(e).

3. Incremental Harmonic Balance Method (IHBM)

In this section we consider a case of $e = 1$ and employ IHBM to obtain the Periodic Solutions (PS) of the system described by Eq. (1). For the convenience, let $t = \omega\tau$, and the original system Eq. (1) can be rewritten as

$$\omega^2\ddot{x} + 2\xi\omega\dot{x} + g(x) = a\cos(t), \tag{5}$$

where dot represents the derivative w.r.t. t, and let $q_0(t) = a\cos(t)$.

For system Eq. (5), we assume that $x_0(t)$ is the initial approximate solution corresponding to the excitation parameters ω_0 and q_0. Then its nearby solution is

$$x(t) = x_0(t) + \Delta x(t), \quad \omega = \omega_0 + \Delta\omega, \quad q = q_0 + \Delta q, \tag{6}$$

where $\Delta x(t), \Delta\omega$ and Δq are small increments.

Correspondingly, the piecewise linear function $g(x)$ can be represented as the following first-order Taylor's series expansion,

$$g(x) = g(x_0) + g'(x_0)\Delta x, \tag{7}$$

where $g'(x_0)$ represents the value of the first derivative of $g(x)$ w.r.t. x at x_0.

Substituting Eqs (6) and (7) into Eq. (5) and omitting the nonlinear higher-ordered terms of the small increments, the system Eq. (5) can be rewritten as the following,

$$\omega_0^2\Delta\ddot{x} + 2\xi\omega_0\Delta\dot{x} + g'(x_0)\Delta x = R + S\Delta\omega + \Delta q, \tag{8}$$

where

$$R = -(\omega_0^2\ddot{x_0} + 2\xi\omega_0\dot{x_0} + g(x_0) - q_0), \quad S = -(2\omega_0\ddot{x_0} + 2\xi\dot{x_0}), \tag{9}$$

R is the corrective term which goes to 0 when the solution is reached and S is the unbalanced force term due to unit frequency shifting.

Though Eq. (8) is linear, there is variable coefficient due to piecewise linearity of the elastic force and it is not feasible to be solved directly. Hence we apply the Galerkin procedure in the following way. The initial approximate periodic solution and its small increment may be expressed as

$$x_0 = \frac{c_0}{2} + \sum_{n=1}^{N}\left(c_n\cos(nt) + b_n\sin(nt)\right), \quad \Delta x = \frac{\Delta c_0}{2} + \sum_{n=1}^{N}\left(\Delta c_n\cos(nt) + \Delta b_n\sin(nt)\right), \tag{10}$$

where N is the number of the harmonic terms taken in the truncated Fourier series. Denoting the base functions vector, the coefficients vector and its incremental vector, are expressed by

$$\mathbf{p} = \left(\frac{1}{2}, \cos(t), \cos(2t), \cdots, \cos(Nt), \sin(t), \sin(2t), \cdots, \sin(Nt)\right)^T,$$
$$\mathbf{m} = (c_0, c_1, c_2, \cdots, c_N, b_1, b_2, \cdots, b_N)^T,$$
$$\mathbf{\Delta m} = (\Delta c_0, \Delta c_1, \Delta c_2, \cdots, \Delta c_N, \Delta b_1, \Delta b_2, \cdots, \Delta b_N)^T.$$

Multiplying both of the sides of Eq. (8) respectively with every element of the base functions vector and integrating them from 0 to 2π, the following (2N+1)-dimensional linear algebraic equations with the unknown variables $\Delta c_i, \Delta b_i, i = 0, 1, \cdots, N, j = 1, \cdots, N$ are obtained,

$$\mathbf{C} \cdot \mathbf{\Delta m} = \mathbf{R} + \mathbf{S}\Delta\omega + \mathbf{\Delta Q}, \tag{11}$$

where matrix $\mathbf{C}$ and vectors $\mathbf{R}$, $\mathbf{S}$ and $\mathbf{\Delta Q}$ are presented in Eqs (23)–(32) in Appendix A. The solution is obtained by iterating Eq.(11) as explained in the following section.

4. Period One Impacting Orbits

Period one response is fundamental for most of the operating systems and machinery, therefore its effective computing is essential. Generally, in the study of forced vibration of dynamical systems, the excitation level is kept as constant, thus $\mathbf{\Delta Q} = 0$. We choose increment option for which the frequency increment is prescribed and $\Delta\omega$ is 0 in the subsequent iteration process. Thus Eq. (11) reads as

$$\mathbf{C} \cdot \mathbf{\Delta m} = \mathbf{R}, \tag{12}$$

or

$$\mathbf{\Delta m} = \mathbf{C}^{-1}\mathbf{R}, \tag{13}$$

where $\mathbf{\Delta m}$ is the vector of Δc_i and Δb_i increments and $\mathbf{C}^{-1}$ is the inverse matrix of $\mathbf{C}$. The iteration process is carried out as follows

$$\mathbf{C}^k \cdot \mathbf{\Delta m}^{k+1} = \mathbf{R}^k, \quad \mathbf{m}^{k+1} = \mathbf{m}^k + \mathbf{\Delta m}^{k+1},$$

where the updated matrices $\mathbf{C}^{k+1}, \mathbf{R}^{k+1}$ are then evaluated from Eqs (24)–(29) which only depend on the iterations of the coefficients b_n and c_n with $b_n^{k+1} = b_n^k + \triangle b_n^k$, $c_n^{k+1} = c_n^k + \triangle c_n^k$, $n = 0, 1, \cdots, N, k \in Z^+$. When the norm of $\mathbf{\Delta m}^k$, i.e., $\mathrm{Abs}_{max}(\mathbf{\Delta m}^k)$ becomes sufficiently small, e.g., less than 10^{-16}, then the corresponding b_n^k and c_n^k are considered to be constant. The converged coefficients b_n^k and c_n^k obtained in the result of this process are substituted in Eq. (10) to generate approximate periodic solution $x_0(t)$. The details of this derivation are presented in Appendix A.

Here we consider the second order approximation, $N = 2$, and in Table 1 we present the computed coefficients b and c for two different system parameters values. Examining the second and third row of Table 1, it is clear we have obtained two different periodic orbits shown in Fig. 2 for the same parameters $\xi = 0.19884, a = 0.1, \omega = 0.3, e = 1$, which means co-existing attractors (bi-stability).

Table 1: Amplitude components by the IHBM for the second order harmonics.

ξ	a	ω_0	c_0	c_1	b_1	c_2	b_2
0.020000	0.500000	1	0	-0.499201	0.019968	0	0
0.19884	0.10000	0.3	0	-0.402983	0.534194	0	0
0.19884	0.10000	0.3	0.272	-0.402983	0.534194	0	0

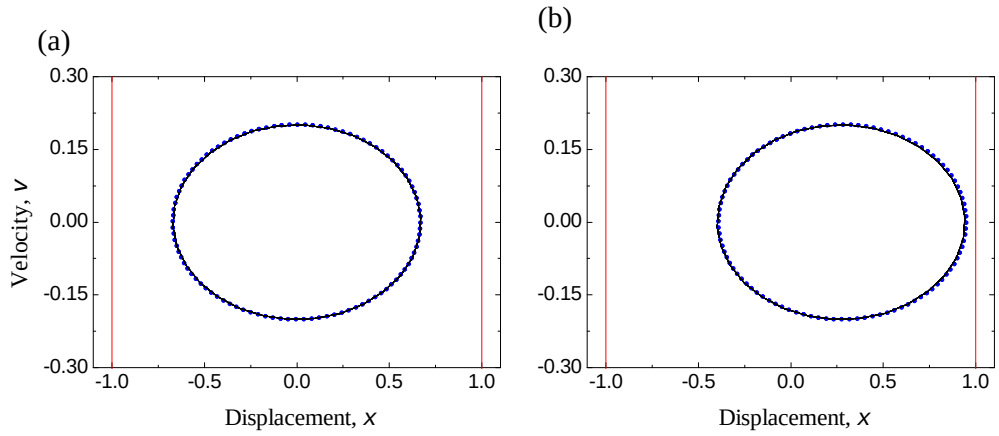

Figure 2: Comparisons of the co-existing responses of the system (1) calculated by IHBM and the numerical simulations, where $\xi = 0.19884$, $e = 1$, $\omega = 0.3$ and $a = 0.1$ for the following initial conditions (a) $x(0) = 0$, $x'(0) = 0$ and (b) $x(0) = -1.87$, $x'(0) = 0$. The blue points are those of the numerical simulations and the black solid lines are those of the IHBM. Red vertical lines denote the discontinuity boundaries.

It should be noted here that infinite number of periodic solutions co-exist in the gap between $-e$ and e. If the mass does not come in contact with any of the constraints, the system becomes linear and the solution depending on the initial conditions $x(0) = x_0$ and $x'(0) = v_0$ can be obtained as

$$x(\tau) = x_0 + \frac{v_0}{2\xi} + \left(\frac{a}{4\xi^2+\omega^2} - \frac{v_0}{2\xi}\right)\exp(-2\xi\tau) + \frac{a}{\omega^2+4\xi^2}\left(-\cos(\omega\tau) + \frac{2\xi}{\omega}\sin(\omega\tau)\right). \quad (14)$$

This means that the centres of such periodic orbits are located at horizontal axis at $x = x_0 + \frac{v_0}{2\xi}$ and the amplitude of the response is $\frac{a}{\omega\sqrt{4\xi^2+\omega^2}}$. These orbits have to fit within the gap, i.e. $|x| < e$ to exist, and therefore the limits for initial conditions and excitation parameters could be evaluated. So we obtain the limitations on the initial displacement and velocity:

$$-e + \frac{a}{4\xi^2+\omega^2} < x_0 + \frac{v_0}{2\xi} < e - \frac{a}{4\xi^2+\omega^2}. \quad (15)$$

Example is shown in Fig. 3 computed for $\xi = 0.13058$, $e = 1$, $\omega = 0.3$ and $a = 0.1$. Fig. 3(a) demonstrates the basins of attractions for multiple non-impacting solutions (one of them is

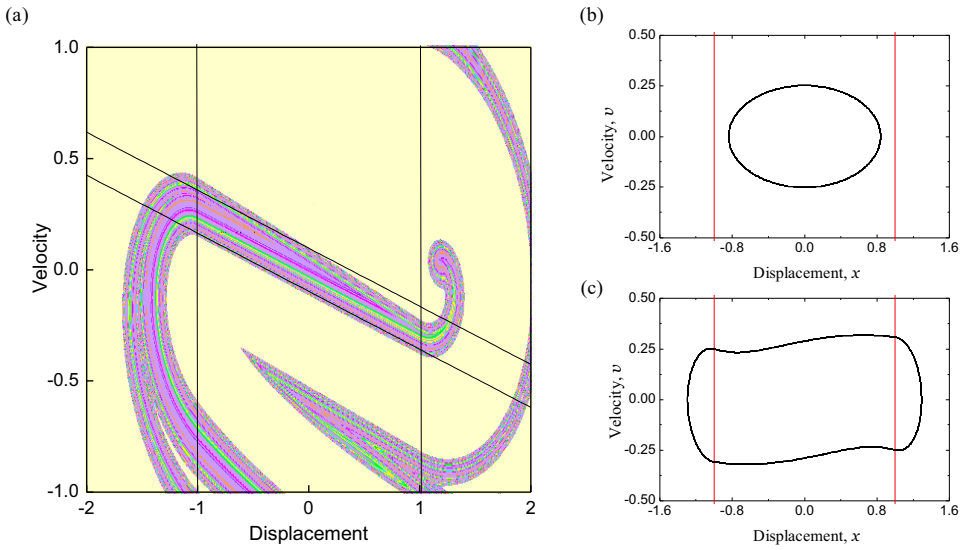

Figure 3: (a) Basins of attraction for multiple co-existing solutions marked in bright colours and computed for $\xi = 0.13058$, $e = 1$, $\omega = 0.3$ and $a = 0.1$. A pair of the vertical lines depicts the discontinuity boundaries whilst the slanted ones indicate the limits described by Eq. (15); (b) trajectory of the non-impacting symmetric solution; (c) trajectory of the impacting solution with light yellow basin.

presented in Fig. 3(b)) and impacting solution shown in Fig. 3(c). Here the vertical lines show the discontinuity boundaries and black lines in Fig. 3(a) indicate the limits described by Eq. (15). As can be seen from Fig. 3(a), although the numerical simulations capture a number of non-impacting solutions, the full complexity of the system can not be described and the results depends significantly on the precision and calculation settings. Examples of basins of attraction calculated for $\xi = 0.19884$, $e = 1$, $\omega = 0.3$ and $a = 0.1$ (case of the multiple non-impacting solutions presented in Table 1) are shown in Fig. 4 where the time step of calculations (characterised by the step per cycle parameter "spc" as specified in the caption of Fig. 4) is smaller in Fig. 4(a) than in Fig. 4(b). Also a different number of initial checks (characterised by maximum checks per initial point parameter "mc") is used to determine the different attractors using mapping techniques in software Dynamics [55]. Figures 4(c) and (d) present samples of multiple co-existing non-impacting solutions. Although a number of solutions is identified by the numerical simulation, there is still a lot of uncertainties in the results and no specific solution was found for the initial conditions within the light yellow basins. For this basin, multiple (infinite number of) solutions co-exist as previously explained.

The accuracy of the IHBM is evaluated here by comparing its results against those obtained from direct numerical simulation, which uses a high accuracy Runge-Kutta scheme with a precise determination of discontinuity occurrences. Figures 5 and 6 compare the steady state solutions computed by the IHBM and marked by the black solid lines with the results of numerical simulations

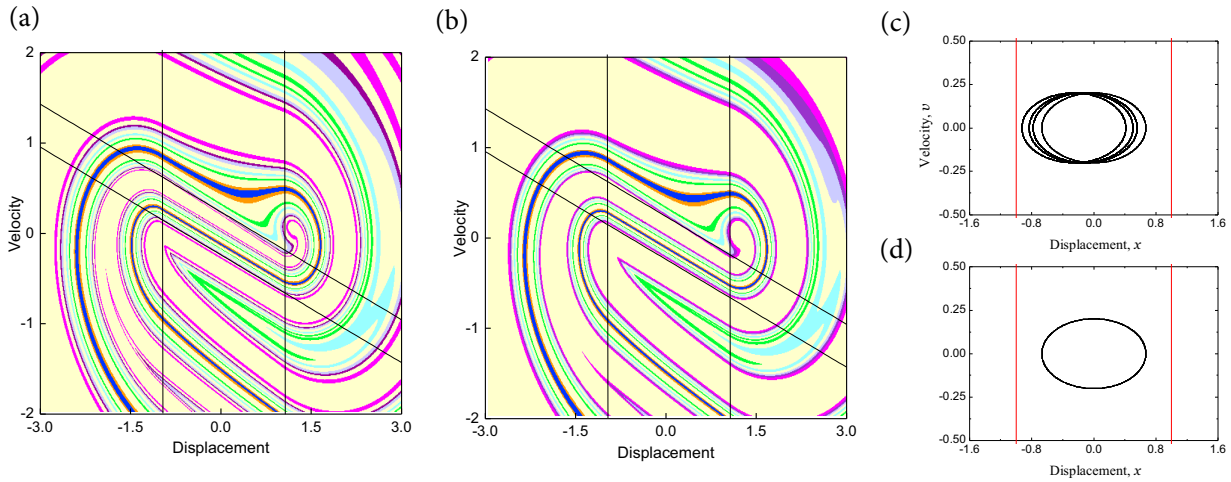

Figure 4: Basins of attraction for multiple co-existing solutions marked in bright colours and computed for $\xi = 0.19844$, $e = 1$, $\omega = 0.3$ and $a = 0.1$. A pair of the vertical lines depicts the discontinuity boundaries whilst the slanted ones indicate the limits described by Eq. (15): (a) spc=500, mc=200 and (b) spc=2000, mc=300. (c) and (d) trajectories of the non-impacting symmetric solutions.

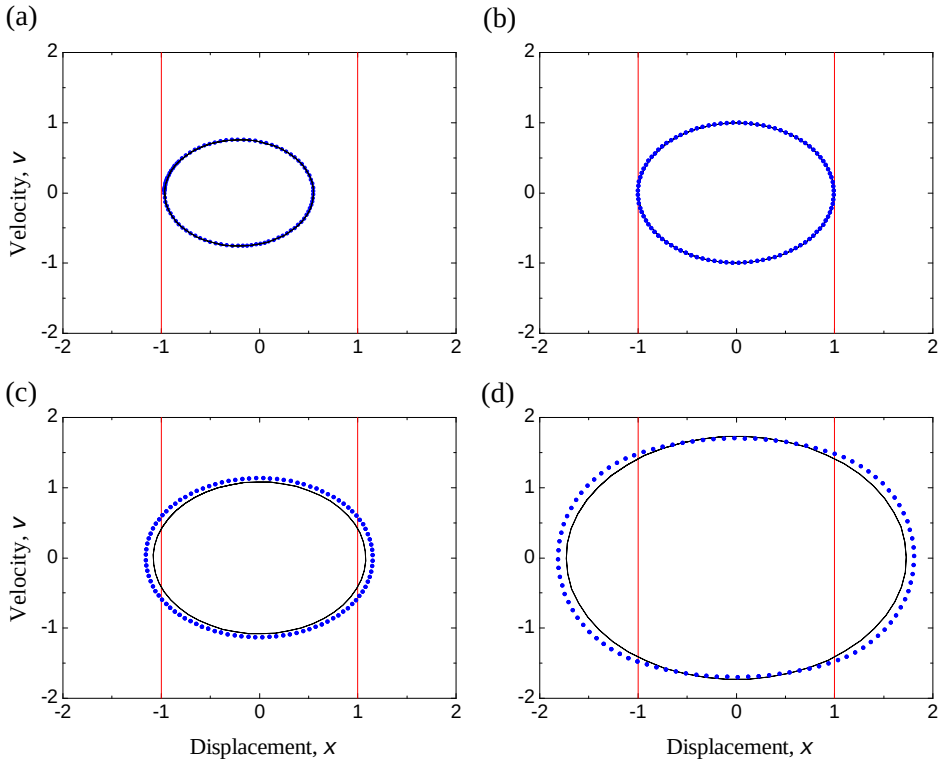

Figure 5: Comparisons of the corresponding phase portraits of the system (1) shown in Fig. 2 calculated by IHBM and the numerical simulations, where $\xi = 0.02$, $e = 1$, $\omega = 1$ and (a) $a = 0.75820$, (b) $a = 0.99814$, (c) $a = 1.08330$, (d) $a = 1.19940$. The blue points are those of the numerical simulations and the black solid lines are those of the IHBM. Red vertical lines denote the discontinuity boundaries.

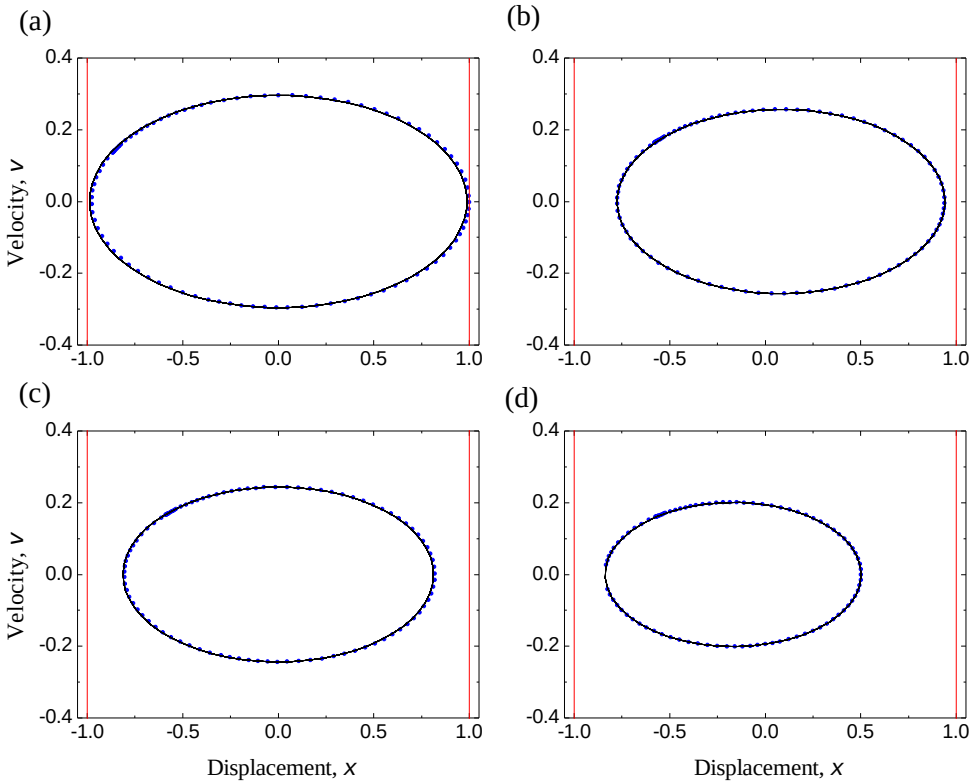

Figure 6: Comparisons of the corresponding phase portraits of the system (1) calculated by IHBM and the numerical simulations, where $a = 0.1$, $e = 1$, $\omega = 0.3$ and (a) $\xi = 0.07754$, (b) $\xi = 0.12395$, (c) $\xi = 0.13994$, (d) $\xi = 0.19884$. The blue points are those of the numerical simulations and the black solid lines are those of the IHBM. Red vertical lines denote the discontinuity boundaries.

[27] as blue discrete points. Period one motions, including not only the non-impacting orbits as shown in Figs 5a, 6b, 6c and 6d, but also the grazing orbits shown in Figs 5b and 6a, and impacting orbits presented in Figs 5c and 5d are computed successfully.

5. Complex Impacting Periodic Solutions via Harmonic Balance with Alternating Frequency and Time

When using the IHBM, some complex impacting periodic solutions cannot be easily computed. However this can be overcome with the method of Harmonic Balance with Alternating Frequency and Time (HB-AFT). There are significant differences between IHB and HB-AFT methods, which are used for strongly nonlinear systems. In essence the IHBM develops the periodic solution (PS) by incrementing the frequency and amplitude using the linear terms of Taylor's expansion, which leads to the main problem. The Taylor's expansion has certain constraints to ensure its validity, specifically, the smoothness of the function being approximated. This is fine for smooth nonlinear systems (e.g. Duffing oscillator), but for the non-smooth system, a such condition simply does

not hold. In contrast, when applying the HB-AFT method, the smoothness is not required and once we assume that the solution is periodic, the frequencies and amplitudes of the harmonics of these complex periodic solutions can be easily determined by using Discrete Fourier Transformation (DFT).

In the HB-AFT method, first $x(t)$ and the nonlinear part can be written as two groups of Fourier series expansions with the same orthogonal basis. According to system (1), one can get an implicit nonlinear algebraic relationship between the harmonic coefficients of $x(t)$ and the nonlinear part. Then with the help of the Discrete Fourier Transform (DFT) and the Inverse Discrete Fourier Transform (IDFT), the information used to iterate the implicitly algebraic can be obtained. Thus, it can be easily seen that the HB-AFT method is different from the IHBM. It establishes relationships for each order harmonic term directly from the discrete time frequency features, and there is little integration and analytical work required during the solving process of the HB-AFT method. Thus, this method can be considered to be more versatile for the strong nonlinear problems with piecewise linearity. The detailed formulation is presented in Appendix B.

The accuracy of the HB-AFT is evaluated here by comparing its results against those of the numerical analysis of the global dynamics of the piecewise linear oscillator with a play in [27]. Figures 7–9 compare the corresponding steady state solutions computed by the HB-AFT denoted by the black solid lines with the results of direct numerical simulation [27], which are presented by blue discrete points at the same phase planes, showing great accuracy. Complex impacting period one motions presented in [27] (see Figs 4d and 4e, Figs 5a and 5b and Figs 9b, 9c, 9d and 9f in [27]) are computed successfully as can be seen from Figs 7–9.

The generic explicit expression of the system (1) for HB-AFT is the following,

$$x(t) = \frac{e_0}{2} + \sum_{n=1}^{N} (e_n \cos((2n-1)t) + d_n \sin((2n-1)t)). \tag{16}$$

Its corresponding expression of $y(t)$ can be obtained by assuming $y(t) = \omega \dot{x}(t)$. The coefficients of formula Eq. (16) used to compute Figs 7–9 of system (1) by the HB-AFT are listed in Table 2, where the parameters ω, e, ξ, a are presented in the captions of Figs 7–9 and $e_0 = 0$ for all cases.

As can be seen from Figs 7 – 9, for $N = 6$ complex trajectories with impacts and internal sub-loops could be approximated well by the HB-AFT method. It should be noted here that no co-exiting solutions were found for the parameter values from Figs 7, 8a and 9a, 9b, 9c. However multiple non-impacting solutions co-exist with one impacting period-1 response for the parameters from Figs 8b and 9d as discussed above, and their basins of attractions are presented in Figs 3 and 10, respectively.

Table 2: Amplitude components of the explicit expression Eq. (16) used to compute by HB-AFT Figs 7–9 for $N = 6$.

Figures	e_1	e_2	e_3	e_4	e_5	e_6
Fig.7(a)	-1.145600	-0.005700	-0.001300	-0.000200	0	0
Fig.7(b)	-1.779500	-0.028000	0.000500	0.000700	0	0
Fig.8(a)	1.090000	0.068600	-0.021900	0	0	0
Fig.8(b)	0.104900	-0.079500	0.023500	-0.006500	0	0
Fig.9(a)	1.219100	0.252000	-0.108600	-0.120800	-0.085400	-0.032400
Fig.9(b)	1.065300	0.338900	0.164700	0.087900	0	0
Fig.9(c)	0.688800	-0.148600	0.002800	0	0	0
Fig.9(d)	-0.353500	0.030600	-0.007200	-0.00100	0	0

Figures	d_1	d_2	d_3	d_4	d_5	d_6
Fig.7(a)	0.048600	0.000800	0.000300	0.000100	0	0
Fig.7(b)	0.106200	0.005500	-0.000200	-0.000300	0	0
Fig.8(a)	0.578000	0.181100	0.035100	0	0	0
Fig.8(b)	1.151600	-0.078100	0.014000	-0.0014000	0	0
Fig.9(a)	0.870800	-0.274400	-0.150300	-0.007400	0.005200	0.012500
Fig.9(b)	1.001900	-0.075900	-0.115100	0.007400	0	0
Fig.9(c)	1.342900	0.059900	-0.018800	0	0	0
Fig.9(d)	1.366300	-0.070500	0.005400	-0.000100	0	0

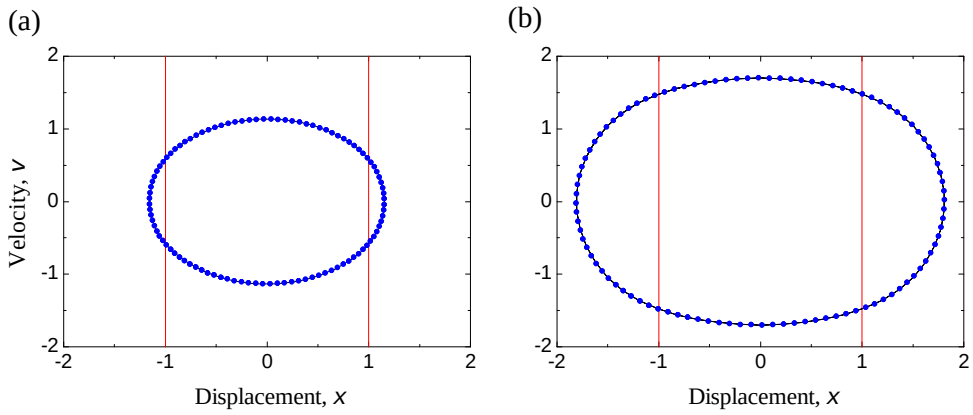

Figure 7: Comparison of the corresponding phase portraits in Fig. 4 (respectively d and e) in [27] of the system (1) by HB-AFT and the numerical simulations, where $\omega = 1$, $e = 1$, $\xi = 0.02$ and (a) $a = 1.08330$, (b) $a = 1.19940$. The blue points are those of the numerical simulations and the black solid line is that of the HB-AFT. Red vertical lines denote the discontinuity boundaries.

6. Conclusions

Two Harmonic Balance based methods, namely the method of Incremental Harmonic Balance (IHBM) and the method of Harmonic Balance with Alternating Frequency and Time (HB-AFT) are

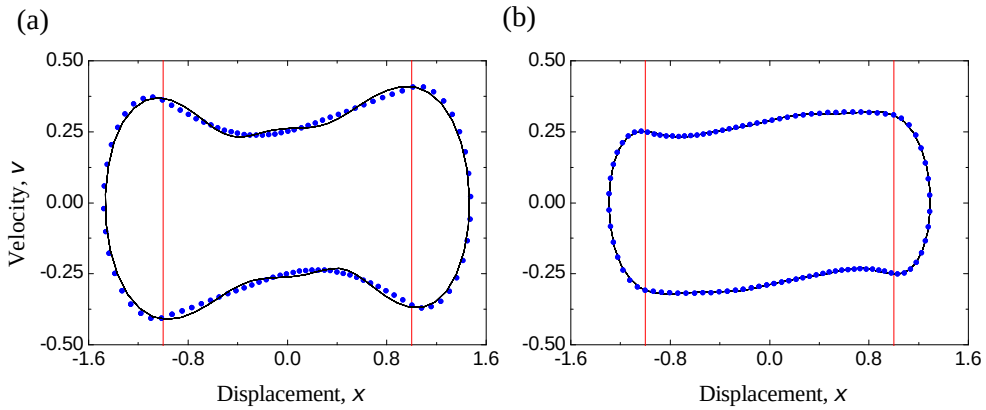

Figure 8: Comparison of the corresponding phase portraits in Fig. 5 (respectively a and b) in [27] of the system (1) by HB-AFT and the numerical simulations, where $\omega = 0.3, e = 1, a = 0.1$ and (a) $\xi = 0.05063$, (b) $\xi = 0.13058$. The blue points are those of the numerical simulations and the black solid line is that of the HB-AFT. Red vertical lines denote the discontinuity boundaries.

successfully employed to analyze dynamics of the piecewise linear oscillator with a play investigated in [27]. Computations of periodic responses for this non-smooth system were effectively carried out using the IHB and HB-AFT methods for various values of the system parameters. Periodic orbits, including not only the non-impacting, but also the grazing and impacting, were effectively determined. Increasing number of terms in the HB-AFT approximation allows to compute more complex impacting trajectories including those with internal sub-loops in the contact regions.

It was found that an infinite number of non-impacting solutions can co-exist in the gap where mass is not in contact with the spring and the approximate boundaries of the region on the phase plane for such cases were determined analytically. It was shown that the numerically computed basins of attraction correspond well to the established boundaries described by Eq.(15).

The obtained good agreements with the direct numerical integration results confirm robustness of the applied Harmonic Balance based methods, which can be used to study global dynamics of non-smooth systems.

Acknowledgments

The authors would like to acknowledge the financial support by NNSF of China (Nos. 11372282 and 10702065) and Scholarship of China; The National Secretariat of Science, Technology and Innovation of Ecuador (SENESCYT); The Escuela Superior Politcnica del Litoral of Ecuador (ESPOL).

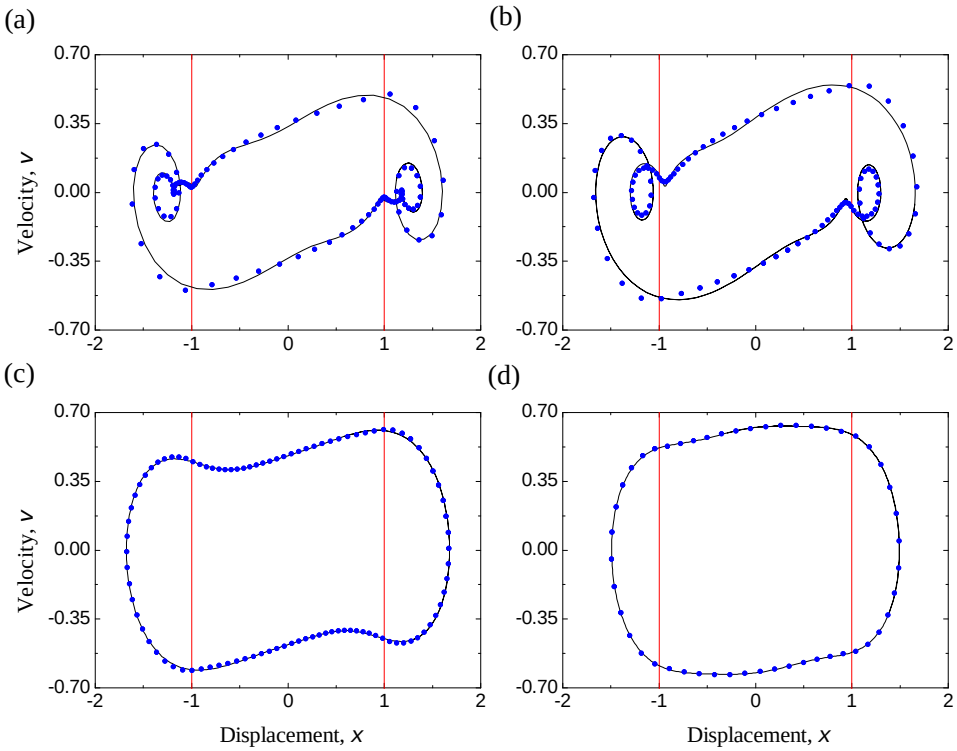

Figure 9: Comparison of the corresponding phase portraits in Fig. 9 (respectively b, c, d and f) in [27] of the system (1) by HB-AFT and the numerical simulations, where $a = 0.3, e = 1, \xi = 0.2$ and (a) $\omega = 0.11246$, (b) $\omega = 0.16260$, (c) $\omega = 0.40022$, (d) $\omega = 0.50050$. The blue points are those of the numerical simulations and the black solid line is that of the HB-AFT. Red vertical lines denote the discontinuity boundaries.

Appendix A

In this appendix, the detailed process of the Eq. (11) is presented here due to its length and tediousness. Substituting Eq. (10) into Eq. (8), then multiplying it by $\frac{1}{2}$ and integrating it from 0 to 2π, it follows that

$$\begin{aligned}
&\int_0^{2\pi} \frac{1}{2}\left(\omega_0^2\Delta\ddot{x} + 2\xi\omega_0\Delta\dot{x} + g'(x_0)\Delta x\right)dt = \int_0^{2\pi} \frac{1}{2}\left(\omega_0^2\left(\sum_{n=1}^{N} -n^2\left(\Delta c_n\cos(nt) + \Delta b_n\sin(nt)\right)\right)\right. \\
&\left. +2\xi\omega_0\left(\sum_{n=1}^{N} -n(\Delta c_n\sin(nt) - \Delta b_n\cos(nt))\right) + g'(x_0)\left(\frac{\Delta c_0}{2} + \sum_{n=1}^{N}(\Delta c_n\cos(nt) + \Delta b_n\sin(nt))\right)\right)dt \\
&= \frac{\Delta c_0}{4}\int_0^{2\pi} g'(x_0)dt + \frac{1}{2}\sum_{n=1}^{N}\Delta c_n\int_0^{2\pi} g'(x_0)\cos(nt)dt + \frac{1}{2}\sum_{n=1}^{N}\Delta b_n\int_0^{2\pi} g'(x_0)\sin(nt)dt, \qquad (17)
\end{aligned}$$

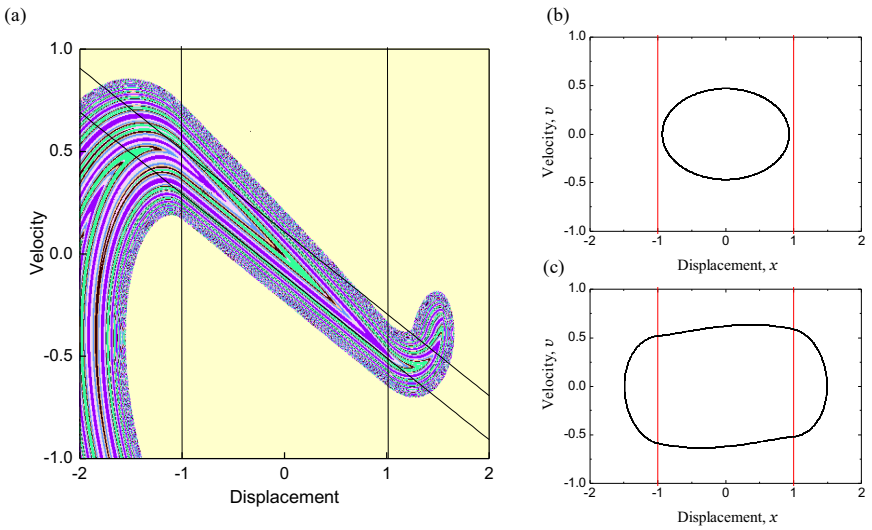

Figure 10: (a) Example of basins of attraction for multiple co-existing solutions marked in bright colours and computed for $\xi = 0.2$, $e = 1$, $\omega = 0.5005$ and $a = 0.3$. A pair of the vertical lines depicts the discontinuity boundaries whilst the slanted ones indicate the limits described by Eq. (15); (b) trajectory of the non-impacting symmetric solution; (c) trajectory of the impacting solution with light yellow basin.

$$\int_0^{2\pi} \frac{1}{2}\left(R + S\Delta\omega + \Delta q\right) dt = \int_0^{2\pi} \frac{1}{2}\left(-\left(\omega_0^2\left(\sum_{n=1}^{N} -n^2(c_n\cos(nt) + b_n\sin(nt))\right)\right.\right.$$
$$+2\xi\omega_0\left(\sum_{n=1}^{N} -n(c_n\sin(nt) - b_n\cos(nt))\right) + g(x_0) - a\cos(t)\Bigg) - \Bigg(2\omega_0\left(\sum_{n=1}^{N} -n^2(c_n\cos(nt) + b_n\sin(nt))\right)$$
$$\left.\left.+2\xi\left(\sum_{n=1}^{N} -n(c_n\sin(nt) - b_n\cos(nt))\right)\right)\Delta\omega + \Delta a\cos(t)\right) dt$$
$$= -\frac{1}{2}\int_0^{2\pi} g(x_0)dt, \tag{18}$$

$\Delta q = \cos(t)\Delta a$ due to $q_0(t) = a\cos(t)$ and Eq.(6).

Multiplying Eq. (8) by $\cos(it), i = 1, \cdots, N$ and integrating it from 0 to 2π, it follows that

$$\int_0^{2\pi} \cos(it)\left(\omega_0^2\Delta\ddot{x} + 2\xi\omega_0\Delta\dot{x} + g'(x_0)\Delta x\right) dt =$$
$$= -\omega_0^2 i^2\Delta c_i\pi + 2\xi\omega_0 i\Delta b_i\pi + \frac{\Delta c_0}{2}\int_0^{2\pi} g'(x_0)\cos(it)dt + \sum_{n=1}^{N}\Delta c_n\int_0^{2\pi} g'(x_0)\cos(it)\cos(nt)dt$$
$$+\sum_{n=1}^{N}\Delta b_n\int_0^{2\pi} g'(x_0)\cos(it)\sin(nt)dt, \tag{19}$$

$$\int_0^{2\pi} \cos(it)\,(R + S\Delta\omega + \Delta q)\,dt = \tag{20}$$
$$= \omega_0^2 i^2 c_i \pi - 2\xi\omega_0 i b_i \pi - \int_0^{2\pi} g(x_0)\cos(it)dt + a\pi\delta_{1,i} + (2\omega_0 i^2 c_i\pi - 2\xi i b_i \pi)\Delta\omega + \Delta a\pi\delta_{1,i},$$

where $\delta_{i,j} = \begin{cases} 1, & for \quad i = j, \\ 0, & else \end{cases}$ is the Kronecker function.

Multiplying Eq. (8) by $\sin(it), i = 1, \cdots, N$ and integrating it from 0 to 2π, it follows that

$$\int_0^{2\pi} \sin(it)\left(\omega_0^2\Delta\ddot{x} + 2\xi\omega_0\Delta\dot{x} + g'(x_0)\Delta x\right)dt = \tag{21}$$
$$= -\omega_0^2 i^2 \Delta b_i \pi - 2\xi\omega_0 i\Delta c_i\pi + \frac{\Delta c_0}{2}\int_0^{2\pi} g'(x_0)\sin(it)dt + \sum_{n=1}^{N}\Delta c_n\int_0^{2\pi} g'(x_0)\sin(it)\cos(nt)dt$$
$$+ \sum_{n=1}^{N}\Delta b_n\int_0^{2\pi} g'(x_0)\sin(it)\sin(nt)dt,$$

$$\int_0^{2\pi} \sin(it)\,(R + S\Delta\omega + \Delta q)\,dt = \tag{22}$$
$$= \omega_0^2 i^2 b_i \pi + 2\xi\omega_0 i c_i\pi - \int_0^{2\pi} g(x_0)\sin(it)dt + (2\omega_0 i^2 b_i\pi + 2\xi i c_i\pi)\Delta\omega.$$

In Eq. (11), the matrix and vectors are defined as follows:

$$\mathbf{C} = \begin{bmatrix} \mathbf{C}_{11} & \mathbf{C}_{12} \\ \mathbf{C}_{21} & \mathbf{C}_{22} \end{bmatrix},$$

where $\mathbf{C}_{11}, \mathbf{C}_{12}, \mathbf{C}_{21}, \mathbf{C}_{22}$ are respectively $(N+1)\times(N+1), (N+1)\times N, N\times(N+1), N\times N$ – dimensional, and

$$\mathbf{R} = \begin{bmatrix} \mathbf{R}_1 \\ \mathbf{R}_2 \end{bmatrix}, \quad \mathbf{S} = \begin{bmatrix} \mathbf{S}_1 \\ \mathbf{S}_2 \end{bmatrix}, \quad \mathbf{\Delta Q} = \begin{bmatrix} \mathbf{\Delta Q}_1 \\ \vartheta \end{bmatrix}, \tag{23}$$

where ϑ is the $(N+1)\times 1$ – dimensional zero vector.

The elements of these matrix and vectors are

$$[\mathbf{C}_{11}]_{ij} = -\delta_{ij}\omega_0^2 j^2\pi + \alpha_i\alpha_j\int_0^{2\pi} g'(x_0)\cos(it)\cos(jt)dt, \quad i,\ j = 0, 1, \cdots, N, \tag{24}$$

which are the coefficients of $\triangle c_j$, where $\alpha_j = \begin{cases} 1, & for \quad j \neq 0, \\ \frac{1}{2}, & for \quad j = 0. \end{cases}$

$$[\mathbf{C}_{12}]_{ij} = 2\delta_{ij}\xi\omega_0 j\pi + \alpha_i\int_0^{2\pi} g'(x_0)\cos(it)\sin(jt)dt, \quad i = 0, 1, \cdots, N,\ j = 1, \cdots, N, \tag{25}$$

which are the coefficients of $\triangle b_j$.

$$[\mathbf{C}_{21}]_{ij} = -2\delta_{ij}\xi\omega_0 j\pi + \alpha_j \int_0^{2\pi} g'(x_0)\sin(it)\cos(jt)dt, \quad i = 1, \cdots, N,\ j = 0, 1, \cdots, N, \tag{26}$$

which are the coefficients of $\triangle c_j$.

$$[\mathbf{C}_{22}]_{ij} = -\delta_{ij}\omega_0^2 j^2\pi + \int_0^{2\pi} g'(x_0)\sin(it)\sin(jt)dt, \quad i, j = 1, \cdots, N, \tag{27}$$

which are the coefficients of $\triangle b_j$. And

$$[\mathbf{R}_1]_i = (\omega_0^2 c_i\pi i^2 - 2\xi\omega_0 i b_i\pi) + \delta_{1i}a\pi - \alpha_i \int_0^{2\pi} g(x_0)\cos(it)dt, \quad i = 0, 1, \cdots, N. \tag{28}$$

$$[\mathbf{R}_2]_i = (\omega_0^2 b_i\pi i^2 + 2\xi\omega_0 i c_i\pi) - \int_0^{2\pi} g(x_0)\sin(it)dt, \quad i = 1, \cdots, N. \tag{29}$$

$$[\mathbf{S}_1]_i = (2\omega_0 c_i\pi i^2 - 2\xi i b_i\pi), \quad i = 0, 1, \cdots, N. \tag{30}$$

$$[\mathbf{S}_2]_i = (2\omega_0 b_i\pi i^2 + 2\xi i c_i\pi), \quad i = 1, \cdots, N. \tag{31}$$

$$[\mathbf{\Delta Q}_1]_i = \delta_{1i}\Delta a\pi, \quad i = 0, 1, \cdots, N, \tag{32}$$

where $\mathbf{R}, \mathbf{S}$ only depend on the coefficients b_n and c_n and they can be re-calculated at each iteration with $b_n^{k+1} = b_n^k + \Delta b_n^k$, $c_n^{k+1} = c_n^k + \Delta c_n^k$, $n = 0$ *or* $1, \cdots, N, k \in Z^+$.

The computation of the nonlinear parts in Eqs (24–29), i.e., the integration parts, needs to know the roots of the equation $|x_0(\theta)| = 1$, where $x_0(\theta)$ is the initial approximate solution corresponding to the excitation parameters ω_0 and q_0 in Eq. (6) and Eq. (10). In the computer program, this is achieved at each iteration through a procedure which uses bisection and interpolation methods on the trigonometric equation $|x_0(\theta)| = 1$. These roots belonging to the interval between $\theta_0 = 0$ and $\theta_{M+1} = 2\pi$, are $\theta_1 < \theta_2 < \cdots < \theta_M$.

To simplify computation of the nonlinear integration parts, we define two functions $S_{m,n}$ and $H(x, y)$ to express the functions $g(x_0)$ and $g'(x_0)$ in different intervals ($m = 1, 2, ..., M + 1$ and $n = -2, -1, 0, 1$). The step function $H(x, y)$ is

$$H(x, y) = \begin{cases} 1, & for \quad xy < 0, \\ 0, & for \quad xy > 0. \end{cases} \tag{33}$$

And function $S_{m+1,n} = \text{sign}(x_0(\theta) - e_n), \theta \in [\theta_m, \theta_{m+1}]$. Then $S_{1,n}, S_{2,n}, \cdots, S_{M+1,n}$ be the sign functions of the functions $x_0(\theta) - e_n$, where for the four specified values of n we have $e_{-2} =$

$-\infty$, $e_{-1} = -1$, $e_0 = 1$ and $e_1 = +\infty$. The subscript indexes n of the non-differentiable points of the piecewise linear non-dimensional function $g(x)$ (Eq. (2)) are $n = -1$ and 0. For example, $x_0(\theta) + 1$ corresponds to $n = -1$, i.e., $e_{-1} = -1$ and $x_0 - 1$ corresponds to $n = 0$, i.e., $e_0 = 1$.

$H(S_{u+1,v_0}, S_{u+1,v_0+1}) = 1$ means that by the definition of function $S_{m,n}$ we have $\theta \in [\theta_u, \theta_{u+1}]$ since the first subscript indexes of both S_{u+1,v_0} and S_{u+1,v_0+1} are same. Since $H(S_{u+1,v_0}, S_{u+1,v_0+1}) = 1$, so $S_{u+1,v_0} S_{u+1,v_0+1} < 0$, and since $S_{u+1,v_0} > S_{u+1,v_0+1}$, so it must hold that $S_{u+1,v_0} > 0 > S_{u+1,v_0+1}$, i.e., $x_0(\theta) \in [e_{v_0}, e_{v_0+1}]$. Since there are only two non-differentiable points $e_{-1} = -1$ and $e_0 = 1$ in this paper, for any interval $[\theta_u, \theta_{u+1}]$, it must satisfies that $|x_0(\theta_u)| = |x_0(\theta_{u+1})| = 1$ and only the following three cases hold, $x_0(\theta) > 1, \theta \in (\theta_u, \theta_{u+1})$, $x_0(\theta) < -1, \theta \in (\theta_u, \theta_{u+1})$ or $-1 < x_0(\theta) < 1, \theta \in (\theta_u, \theta_{u+1})$. So in any interval (θ_u, θ_{u+1}), it holds that $g(x_0) = x_0 + 1, g'(x_0) = 1$, or $g(x_0) = x_0 - 1, g'(x_0) = 1$, or $g(x_0) = g'(x_0) = 0$.

For any integration interval (θ_u, θ_{u+1}), the nonlinear part can be expressed as the following,

$$\int_{\theta_u}^{\theta_{u+1}} g'(x_0)\cos(it)\cos(jt)dt = (H(S_{u+1,-2}, S_{u+1,-1}) \cdot 1 + H(S_{u+1,-1}, S_{u+1,0}) \cdot 0 \quad (34)$$
$$+ H(S_{u+1,0}, S_{u+1,1}) \cdot 1) \int_{\theta_u}^{\theta_{u+1}} \cos(it)\cos(jt)dt,$$

where $\cdot$ is the multiplication sign. This can be proved in the following way. For the last case $-1 < x_0(\theta) < 1, \theta \in (\theta_u, \theta_{u+1})$, it follows that $H(S_{u+1,-1}, S_{u+1,0}) = 1$, $H(S_{u+1,-2}, S_{u+1,-1}) = H(S_{u+1,0}, S_{u+1,1}) = 0$, so $H(S_{u+1,-2}, S_{u+1,-1}) \cdot 1 + H(S_{u+1,-1}, S_{u+1,0}) \cdot 0 + H(S_{u+1,0}, S_{u+1,1}) \cdot 1 = 0$. It is consistent with that $g'(x_0) = 0$ for $-1 < x_0(\theta) < 1, \theta \in (\theta_u, \theta_{u+1})$. It also holds for the other two cases. For the first case $1 < x_0(\theta), \theta \in (\theta_u, \theta_{u+1})$, it follows that $H(S_{u+1,0}, S_{u+1,1}) = 1$, $H(S_{u+1,-2}, S_{u+1,-1}) = H(S_{u+1,-1}, S_{u+1,0}) = 0$, so $H(S_{u+1,-2}, S_{u+1,-1}) \cdot 1 + H(S_{u+1,-1}, S_{u+1,0}) \cdot 0 + H(S_{u+1,0}, S_{u+1,1}) \cdot 1 = 1$. It is consistent with that $g'(x_0) = 1$ for $1 < x_0(\theta), \theta \in (\theta_u, \theta_{u+1})$. For the second case $x_0(\theta) < -1, \theta \in (\theta_u, \theta_{u+1})$, it follows that $H(S_{u+1,-2}, S_{u+1,-1}) = 1$, $H(S_{u+1,0}, S_{u+1,1}) = H(S_{u+1,-1}, S_{u+1,0}) = 0$, so $H(S_{u+1,-2}, S_{u+1,-1}) \cdot 1 + H(S_{u+1,-1}, S_{u+1,0}) \cdot 0 + H(S_{u+1,0}, S_{u+1,1}) \cdot 1 = 1$. It is consistent with that $g'(x_0) = 1$ for $x_0(\theta) < -1, \theta \in (\theta_u, \theta_{u+1})$. So the above formula (34) is proved.

Let $e_{-2} = -\infty, e_{-1} = -1, e_0 = 1, e_1 = +\infty$. Then the nonlinear parts of (24-29) can be obtained as the following,

$$[\mathbf{C}_{11}]_{ij}^{NL} = \alpha_i \alpha_j \int_0^{2\pi} g'(x_0)\cos(it)\cos(jt)dt \quad (35)$$
$$= \alpha_i \alpha_j \sum_{u=0}^{M} ((H(S_{u+1,-2}, S_{u+1,-1}) \cdot 1 + H(S_{u+1,-1}, S_{u+1,0}) \cdot 0$$
$$+ \quad H(S_{u+1,0}, S_{u+1,1}) \cdot 1)(A_{ij}(\theta_{u+1}) - A_{ij}(\theta_u)))$$
$$= \alpha_i \alpha_j \sum_{u=0}^{M} ((H(S_{u+1,-2}, S_{u+1,-1}) + H(S_{u+1,0}, S_{u+1,1}))(A_{ij}(\theta_{u+1}) - A_{ij}(\theta_u))),$$

where

$$A_{ij}(\theta) = \begin{cases} \frac{1}{2}(\frac{\sin((i-j)\theta)}{i-j} + \frac{\sin((i+j)\theta)}{i+j}), & for \quad i \neq j, \\ \frac{\theta}{2} + \frac{\sin(2i\theta)}{4i}, & for \quad i = j \neq 0 \\ \theta, & for \quad i = j = 0. \end{cases}$$

$$[\mathbf{C}_{12}]_{ij}^{NL} = \alpha_i \int_0^{2\pi} g'(x_0)\cos(it)\sin(jt)dt \tag{36}$$
$$= \alpha_i \sum_{u=0}^{M}((H(S_{u+1,-2}, S_{u+1,-1}) + H(S_{u+1,0}, S_{u+1,1}))(B_{ij}(\theta_{u+1}) - B_{ij}(\theta_u))),$$

where

$$B_{ij}(\theta) = \begin{cases} \frac{1}{2}(\frac{\cos((j-i)\theta)}{i-j} - \frac{\cos((i+j)\theta)}{i+j}), & for \quad i \neq j, \\ -\frac{\cos(2i\theta)}{4i}, & for \quad i = j. \end{cases}$$

$$[\mathbf{C}_{21}]_{ij}^{NL} = \alpha_j \int_0^{2\pi} g'(x_0)\sin(it)\cos(jt)dt \tag{37}$$
$$= \alpha_j \sum_{u=0}^{M}((H(S_{u+1,-2}, S_{u+1,-1}) + H(S_{u+1,0}, S_{u+1,1}))(B_{ji}(\theta_{u+1}) - B_{ji}(\theta_u))).$$

$$[\mathbf{C}_{22}]_{ij}^{NL} = \int_0^{2\pi} g'(x_0)\sin(it)\sin(jt)dt \tag{38}$$
$$= \sum_{u=0}^{M}((H(S_{u+1,-2}, S_{u+1,-1}) + H(S_{u+1,0}, S_{u+1,1}))(D_{ij}(\theta_{u+1}) - D_{ij}(\theta_u))),$$

where

$$D_{ij}(\theta) = \begin{cases} \frac{1}{2}(\frac{\sin((j-i)\theta)}{j-i} - \frac{\sin((i+j)\theta)}{i+j}), & for \quad i \neq j, \\ \frac{\theta}{2} - \frac{\sin(2i\theta)}{4i}, & for \quad i = j. \end{cases}$$

$$[\mathbf{R}_1]_i^{NL} = -\alpha_i \int_0^{2\pi} g(x_0)\cos(it)dt \tag{39}$$
$$= -\alpha_i \sum_{u=0}^{M} \int_{\theta_u}^{\theta_{u+1}} ((H(S_{u+1,-2}, S_{u+1,-1})(\sum_{n=0}^{N} \alpha_n c_n \cos(nt) + \sum_{n=1}^{N} \alpha_n b_n \sin(nt) + 1)$$
$$+H(S_{u+1,0}, S_{u+1,1})(\sum_{n=0}^{N} \alpha_n c_n \cos(nt) + \sum_{n=1}^{N} \alpha_n b_n \sin(nt) - 1))\cos(it)dt$$
$$= -\alpha_i \sum_{u=0}^{M}((H(S_{u+1,-2}, S_{u+1,-1}) + H(S_{u+1,0}, S_{u+1,1}))(\sum_{n=0}^{N} \alpha_n c_n (A_{in}(\theta_{u+1}) - A_{in}(\theta_u))$$
$$+\sum_{n=1}^{N} \alpha_n b_n (B_{in}(\theta_{u+1}) - B_{in}(\theta_u))) + (H(S_{u+1,-2}, S_{u+1,-1}) - H(S_{u+1,0}, S_{u+1,1}))(E_i(\theta_{u+1})$$
$$-E_i(\theta_u))),$$

where

$$E_i(\theta) = \begin{cases} \frac{\sin(i\theta)}{i}, & for \quad i \neq 0, \\ \theta, & for \quad i = 0. \end{cases}$$

$$[\mathbf{R}_2]_i^{NL} = -\int_0^{2\pi} g(x_0)\sin(it)dt \tag{40}$$
$$= -\sum_{u=0}^{M}((H(S_{u+1,-2}, S_{u+1,-1}) + H(S_{u+1,0}, S_{u+1,1}))(\sum_{j=0}^{N}\alpha_j c_j(C_{ij}(\theta_{u+1}) - C_{ij}(\theta_u))$$
$$+\sum_{j=1}^{N}\alpha_j b_j(D_{ij}(\theta_{u+1}) - D_{ij}(\theta_u))) + (H(S_{u+1,-2}, S_{u+1,-1}) - H(S_{u+1,0}, S_{u+1,1}))$$
$$\cdot(F_i(\theta_{u+1}) - F_i(\theta_u))),$$

and

$$F_i(\theta) = -\frac{\cos(i\theta)}{i}, i = 1, 2, \cdots, N,$$

and

$$C_{ij}(\theta) = B_{ij}(\theta), i = 0, 1, 2, \cdots, N, j = 1, 2, \cdots, N.$$

Appendix B

The HB-AFT method for the system Eq. (1) included two computational schemes, namely the HB and the AFT.

6.1. HB Scheme

The periodic solution $x(t)$ to the transformed system (5) can be assumed as the following,

$$x(t) = a_{x0} + \sum_{k=1}^{K}(a_{xk}\cos(kt) - b_{xk}\sin(kt)). \tag{41}$$

The nonlinear part $g(x) - a\cos(t)$ can be assumed also as the following,

$$\overline{g}(t) = g(x) - a\cos(t) = c_{x0} + \sum_{k=1}^{K}(c_{xk}\cos(kt) - d_{xk}\sin(kt)), \tag{42}$$

where K presents the number of the harmonic terms in Eqs (41) and (42).

Substituting Eqs (41) and (42) into Eq. (5), balancing the coefficients of each harmonic term, one can obtain the algebraic equations $\widetilde{g} = 0$.

It follows from Eq. (41) that

$$\dot{x}(t) = \sum_{k=1}^{K} k(-a_{xk}\sin(kt) - b_{xk}\cos(kt)), \tag{43}$$

and

$$\ddot{x}(t) = \sum_{k=1}^{K} k^2(-a_{xk}\cos(kt) + b_{xk}\sin(kt)). \tag{44}$$

Substituting (41)-(44) into (5), it follows that

$$\begin{aligned}&\sum_{k=1}^{K} k^2\omega^2(-a_{xk}\cos(kt) + b_{xk}\sin(kt)) + 2\xi\omega\sum_{k=1}^{K} k(-a_{xk}\sin(kt) - b_{xk}\cos(kt)) \\ &+c_{x0} + \sum_{k=1}^{K}(c_{xk}\cos(kt) - d_{xk}\sin(kt)) = 0.\end{aligned} \tag{45}$$

Simplifying it, it follows that

$$c_{x0} + \sum_{k=1}^{K}\left((-k^2\omega^2 a_{xk} - 2\xi\omega n b_{xk} + c_{xk})\cos(kt) + (k^2\omega^2 b_{xk} - 2\xi\omega k a_{xk} - d_{xk})\sin(kt)\right) = 0. \tag{46}$$

The algebraic equation $\widetilde{g} = \theta$ can be obtained. For the constant term, it follows that

$$\widetilde{g}(1) = c_{x0}. \tag{47}$$

For the cosine terms, it follows that

$$\widetilde{g}(2k) = -k^2\omega^2 a_{xk} - 2\xi\omega k b_{xk} + c_{xk}. \tag{48}$$

For the sine terms, it follows that

$$\widetilde{g}(2k+1) = k^2\omega^2 b_{xk} - 2\xi\omega k a_{xk} - d_{xk}. \tag{49}$$

Let

$$\begin{pmatrix} P \\ Q \end{pmatrix}^T = \begin{pmatrix} a_{x0} & a_{x1} & b_{x1} & a_{x2} & b_{x2} & \cdots & a_{xK} & b_{xK} \\ c_{x0} & c_{x1} & d_{x1} & c_{x2} & d_{x2} & \cdots & c_{xK} & d_{xK} \end{pmatrix}^T, \tag{50}$$

where P and Q represent the coefficients of harmonics of solutions and nonlinear terms, respectively. In addition, we add the variable

$$P(2K+2) = 0. \tag{51}$$

Note that the frequency ω is unknown in the above analysis. In order to solve the algebraic equation $\widetilde{g} = \theta$ for the Fourier coefficients and the response frequency ω, we impose a condition on the phase of the first harmonic of the periodic solutions based on the fixed-phase method [53, 54], i.e. $a_{x1} = 0$ or $b_{x1} = 0$.

Take P as unknown variables. According to Eqs (41), (42), (47)-(49), we can find the fixed point P^* of $\widetilde{g}$ by the iteration method. Here, the Newton-Raphson method is employed for the iteration, i.e.,

$$P^{j+1} = P^j - (J^j)^{-1}\widetilde{g}^j, \tag{52}$$

where J is the Jacobian matrix of $\widetilde{g}$, i.e. , $J = \frac{\partial \widetilde{g}}{\partial P}$.

After the process of harmonic balance, the values of Q and J in each step of iterations can be obtained by the alternating frequency/time (AFT) technique.

6.2. AFT Scheme

The values of Q and J in each step of iterations can be obtained by the alternating frequency/time (AFT) technique which are presented as follows.

For a supposed P, we can obtain the discrete value of $x(t)$ employing the Inverse Discrete Fourier Transform (IDFT),

$$x(n) = a_{x0} + \sum_{k=1}^{K}(a_{xk}\cos(\frac{2\pi kn}{N}) - b_{xk}\sin(\frac{2\pi kn}{N})), \tag{53}$$

where $n = 0, 1, \cdots, N$. Here, $x(n)$ denotes the sampled point at the nth discrete time, i.e., $x(n\Delta T)$, where $\Delta T = 2\pi/N$, N is the number of samples in the time domain.

According to Eqs (53) and (42), the nonlinear part $g(x) - a\cos(t)$ can be discretized into

$$\overline{g}(n) = g\left(a_{x0} + \sum_{k=1}^{K}\left(a_{xk}\cos(\frac{2\pi kn}{N}) - b_{xk}\sin(\frac{2\pi kn}{N})\right) - a\cos(\frac{2\pi n}{N})\right). \tag{54}$$

The expressions of Q can be obtained by the discrete values of $g(x)$ in the frequency domain employing the DFT, i.e.,

$$\begin{aligned} c_{x0} &= \frac{1}{N}\sum_{n=0}^{N-1}\overline{g}(n), \\ c_{xk} &= \frac{2}{N}\sum_{n=0}^{N-1}\overline{g}(n)\cos(\frac{2\pi kn}{N}), \\ d_{xk} &= -\frac{2}{N}\sum_{n=0}^{N-1}\overline{g}(n)\sin(\frac{2\pi kn}{N}), \end{aligned} \tag{55}$$

where $k = 1, 2, \cdots, K$.

According to Eqs (47)-(49), (53)-(55) and

$$\begin{aligned}
\widetilde{g}(1) &= c_{x0} = \frac{1}{N}\sum_{n=0}^{N-1} g\left(a_{x0} + \sum_{k=1}^{K}(a_{xk}\cos(\frac{2\pi kn}{N}) - b_{xk}\sin(\frac{2\pi kn}{N}))\right), \qquad (56)\\
\widetilde{g}(2k) &= -\omega^2 k^2 a_{xk} - 2\xi\omega k b_{xk} + \frac{2}{N}\sum_{n=0}^{N-1}(g\left(a_{x0} + \sum_{k=1}^{K}(a_{xk}\cos(\frac{2\pi kn}{N}) - b_{xk}\sin(\frac{2\pi kn}{N}))\right)\\
&- a\cos(\frac{2\pi n}{N}))\cos(\frac{2\pi kn}{N}),\\
\widetilde{g}(2k+1) &= \omega^2 k^2 b_{xk} - 2\xi\omega k a_{xk} + \frac{2}{N}\sum_{n=0}^{N-1}(g\left(a_{x0} + \sum_{k=1}^{K}(a_{xk}\cos(\frac{2\pi kn}{N}) - b_{xk}\sin(\frac{2\pi kn}{N}))\right)\\
&- a\cos(\frac{2\pi n}{N}))\sin(\frac{2\pi kn}{N}),
\end{aligned}$$

the elements of J in Eq. (52) can be deduced into

$$\begin{cases}
\frac{\partial\widetilde{g}(1)}{\partial P(1)} = \frac{\partial\widetilde{g}(1)}{\partial a_{x0}} = \frac{1}{N}\sum_{n=0}^{N-1} g'\left(a_{x0} + \sum_{k=1}^{K}(a_{xk}\cos(\frac{2\pi kn}{N}) - b_{xk}\sin(\frac{2\pi kn}{N}))\right),\\
\frac{\partial\widetilde{g}(1)}{\partial P(2j)} = \frac{\partial\widetilde{g}(1)}{\partial a_{xj}} = \frac{1}{N}\sum_{n=0}^{N-1} g'\left(a_{x0} + \sum_{k=1}^{K}(a_{xk}\cos(\frac{2\pi kn}{N}) - b_{xk}\sin(\frac{2\pi kn}{N}))\right)\cos(\frac{2\pi jn}{N}),\\
\frac{\partial\widetilde{g}(1)}{\partial P(2j+1)} = \frac{\partial\widetilde{g}(1)}{\partial b_{xj}} = -\frac{1}{N}\sum_{n=0}^{N-1} g'\left(a_{x0} + \sum_{k=1}^{K}(a_{xk}\cos(\frac{2\pi kn}{N}) - b_{xk}\sin(\frac{2\pi kn}{N}))\right)\sin(\frac{2\pi jn}{N}),\\
\frac{\partial\widetilde{g}(2k)}{\partial P(1)} = \frac{\partial\widetilde{g}(2k)}{\partial a_{x0}} = \frac{2}{N}\sum_{n=0}^{N-1} g'\left(a_{x0} + \sum_{k=1}^{K}(a_{xk}\cos(\frac{2\pi kn}{N}) - b_{xk}\sin(\frac{2\pi kn}{N}))\right)\cos(\frac{2\pi kn}{N}),\\
\frac{\partial\widetilde{g}(2k)}{\partial P(2j)} = \frac{\partial\widetilde{g}(2k)}{\partial a_{xj}} = -\omega^2 j^2\delta_{j,k} + \frac{2}{N}\sum_{n=0}^{N-1} g'\left(a_{x0} + \sum_{k=1}^{K}(a_{xk}\cos(\frac{2\pi kn}{N}) - b_{xk}\sin(\frac{2\pi kn}{N}))\right)\\
\cos(\frac{2\pi jn}{N})\cos(\frac{2\pi kn}{N}),\\
\frac{\partial\widetilde{g}(2k)}{\partial P(2j+1)} = \frac{\partial\widetilde{g}(2k)}{\partial b_{xj}} = -2\xi\omega j\delta_{j,k} - \frac{2}{N}\sum_{n=0}^{N-1} g'\left(a_{x0} + \sum_{k=1}^{K}(a_{xk}\cos(\frac{2\pi kn}{N}) - b_{xk}\sin(\frac{2\pi kn}{N}))\right)\\
\cos(\frac{2\pi kn}{N})\sin(\frac{2\pi jn}{N}),\\
\frac{\partial\widetilde{g}(2k+1)}{\partial P(1)} = \frac{\partial\widetilde{g}(2k+1)}{\partial a_{x0}} = \frac{2}{N}\sum_{n=0}^{N-1} g'\left(a_{x0} + \sum_{k=1}^{K}(a_{xk}\cos(\frac{2\pi kn}{N}) - b_{xk}\sin(\frac{2\pi kn}{N}))\right)\sin(\frac{2\pi kn}{N}),\\
\frac{\partial\widetilde{g}(2k+1)}{\partial P(2j)} = \frac{\partial\widetilde{g}(2k+1)}{\partial a_{xj}} = -2\xi\omega j\delta_{j,k} + \frac{2}{N}\sum_{n=0}^{N-1} g'\left(a_{x0} + \sum_{k=1}^{K}(a_{xk}\cos(\frac{2\pi kn}{N}) - b_{xk}\sin(\frac{2\pi kn}{N}))\right)\\
\cos(\frac{2\pi jn}{N})\sin(\frac{2\pi kn}{N}),\\
\frac{\partial\widetilde{g}(2k+1)}{\partial P(2j+1)} = \frac{\partial\widetilde{g}(2k+1)}{\partial b_{xj}} = \omega^2 j^2\delta_{j,k} - \frac{2}{N}\sum_{n=0}^{N-1} g'\left(a_{x0} + \sum_{k=1}^{K}(a_{xk}\cos(\frac{2\pi kn}{N}) - b_{xk}\sin(\frac{2\pi kn}{N}))\right)\\
\sin(\frac{2\pi kn}{N})\sin(\frac{2\pi jn}{N}),
\end{cases} \qquad (57)$$

where $k = 1, 2, ..., K$, $g'(u) = \frac{dg(u)}{du}$ and $\delta_{j,k}$ is the Kronecker function in Appendix A.

By combining the processes of HB and AFT, the iterations of Eq. (52) can readily yield P^* in proper accuracy. The procedure of the algorithm is as follows:

Algorithm:	
(i)	For a supposed $P^{(0)}$, the values of $g^{(0)}$ and $J^{(0)}$ are obtained by employing Eqs (47)-(55), respectively.
(ii)	Iterate Eq. (52) once, and we can get the value of $P^{(1)}$.
(iii)	Continue (i) and (ii) until the norm of $P^{(j)} - P^{(j-1)}$ is less than an allowed ϵ.
(iv)	Return the value of $P^{(j)}$ which satisfies (iii).

References

[1] S.W. Shaw and P.J. Holmes, A periodically forced piecewise linear oscillator, Journal of Sound and Vibration 90(1) (1983) 129–155.

[2] M. Kleczka, E. Kreuzer and C. Wilmers, Crisis in mechanical systems, in: Proc. Int. Conf. Nonlinear Dynamics in Engineering, Springer, 1990, 141–148.

[3] A.C.J. Luo and S. Menon, Global chaos in a periodically forced, linear system with a dead-zone restoring force, Chaos, Solitons and Fractals 19 (2004) 1189–1199.

[4] M. Wiercigroch, Bifurcation analysis of harmonically excited linear oscillator with clearance, Chaos, Solitons and Fractals 4(2) (1994) 297–303.

[5] A. Kaharaman and R. Singh, Nonlinear dynamics of a spur gear pair, Journal Sound and Vibration 142(1) (1990) 49–75.

[6] S. Theodossiades and S. Natsiavas, Non-linear dynamics of gear-pair systems with periodic stiffness and backlash, Journal of Sound and Vibration 229(2) (2000) 287–310.

[7] S.L.T. de Souza, I.L. Caldas, R.L. Viana and J.M. Balthazar, Sudden changes in chaotic attractors and transient basins in a model for rattling in gear boxes, Chaos, Solitons and Fractals 21 (2004) 763–772.

[8] S. Natsiavas, Periodic response and stability of oscillators with simetric trilinear restoring force, Journal of Sound and Vibration 134(2) (1989) 315–331.

[9] S. Natsiavas,Analytical Modeling of discrete mechanical systems involving contact, impact, and friction, Applied Mechanics Reviews 71(5) (2019) art. no. 050802.

[10] A.B. Nordmark, Non-periodic motion caused by grazing incidence in an impact oscillator, Journal of Sound and Vibration 145(2) (1991) 279–297.

[11] H. Dankowicz and A.B. Nordmark, On the origin and bifurcations of stick-slip oscillations, Physica D: Nonlinear Phenomena 136(3-4) (2000) 280–302.

[12] J. Molenaar, J.G. De Weger and W. Van De Water, Mappings of grazing-impact oscillators, Nonlinearity 14(2) (2001) 301–321.

[13] H. Dankowicz and X. Zhao, Local analysis of co-dimension-one and co-dimension-two grazing bifurcations in impact microactuators, Physica D 202 (2005) 238–257.

[14] M. di Bernardo, M.I. Feigin, S.J Hogan and M.E. Homer, Local analysis of c-bifurcations in n–dimensional piecewise smooth dynamical systems, Chaos, Solitons and Fractals 10(11) (1999) 1881–1908.

[15] H. Nusse, E. Ott and J. Yorke, Border collision bifurcations: An explanation for observed bifurcation phenomena, Physical Review E 49 (1994) 1073–1076.

[16] S. Banerjee and C. Grebogi, Border collision bifurcations in two-dimensional piecewise smooth maps, Physical Review E 59 (1999) 4052–4061.

[17] M. di Bernardo, C.J. Budd and A.R. Champneys, Normal form maps for grazing bifurcations in n-dimensional piecewise-smooth dynamical systems, Physica D: Nonlinear Phenomena 160(3– 4) (2001) 222–254.

[18] M. di Bernardo, P. Kowalczyk and A.B. Nordmark, Bifurcations of dynamical systems with sliding: Derivation of normal-form mappings, Physica D: Nonlinear Phenomena 170(3–4) (2002) 175–205.

[19] Y. Ma, M. Agarwal and S. Banerjee, Border collision bifurcations in a soft impact system, Physical Letter A 354 (2006) 281–287.

[20] Y. Ma, J. Ing, S. Banerjee, M. Wiercigroch and E. Pavlovskaia, The nature of the normal form map for soft impacting systems, International journal of Nonlinear Mechanics 43 (2008) 504–513.

[21] A. Stensson and A.B. Nordmark, Experimental investigation of some consequences of low velocity impacts in the chaotic dynamics of a mechanical system, Philosophical transactions of Royal Society London A 347 (1994) 439–448.

[22] T.P. Piiroinen, L.N. Virgin and A.R. Champneys, Chaos and Period–Adding: Experimental and Numerical Verification of the Grazing Bifurcation, Journal of Nonlinear science 14 (2004) 383–404.

[23] J. Ing, E. Pavlovskaia and M. Wiercigroch, Dynamics of a nearly symmetrical piecewise linear oscillator close to grazing incidence: modelling and experimental verification, Nonlinear Dynamics 46 (2006) 225–238.

[24] J. Ing, E. Pavlovskaia, M. Wiercigroch and S. Banerjee, Experimental study of impact oscillator with one-sided elastic constraint, Philosophical Transactions of the Royal Society A: Mathematical, Physical and Engineering Sciences 366(1866) (2008) 679–704.

[25] S. Banerjee, J. Ing, E. Pavlovskaia, M. Wiercigroch and R. K. Reddy, Invisible grazings and dangerous bifurcations in impacting systems: The problem of narrow-band chaos, Physical Review E 79 (2009) (037201).

[26] E. Pavlovskaia, J. Ing, M. Wiercigroch and S. Banerjee, Complex dynamics of bilinear oscillator close to grazing, International Journal of Bifurcation and Chaos, 20(11) (2010) 3801–3817.

[27] A. S.E. Chong, Y. Yue, E. Pavlovskaia and M. Wiercigroch, Global Dynamics of a Harmonically Excited Oscillator with a Play: Numerical studies, International Journal of Non-Linear Mechanics 94 (2017) 98–108.

[28] A. S. E. Chong, Numerical modelling and stability analysis of non-smooth dynamical systems via ABESPOL, PhD thesis, University of Aberdeen 2016.

[29] H. Dankowicz and F. Schilder, Recipes for Continuation, SIAM, 2013.

[30] M.-H. Tien, K. D'Souza, Analyzing bilinear systems using a new hybrid symbolic-numeric computational method, Journal of Vibration and Acoustics, Transactions of the ASME 141 (3) (2019) art. no. 31008.

[31] L. Woiwode, N.N. Balaji, J. Kappauf, F. Tubita, L. Guillot, C. Vergez, B. Cochelin, A. Grolet, M. Krack, Comparison of two algorithms for Harmonic Balance and path continuation, Mechanical Systems and Signal Processing 136(2020) art. no. 106503.

[32] L.P. Miguel, R.D.O. Teloli, S. da Silva, Some practical regards on the application of the harmonic balance method for hysteresis models, Mechanical Systems and Signal Processing 143 (2020) art. no. 106842.

[33] Y.S. Choi and S.T. Noah, Forced Periodic Vibration of Unsymmetric Piecewise-Linear Systems, J. Sound Vibration 121(3) (1988) 117–126.

[34] S. Maezawa, H. Kumano and Y. Minakuchi, Forced vibrations in an unsymmetrical piece-wise linear system excited by general periodic force function, Bull. JSME 23 (1980) 68–75.

[35] A.H. Nayfeh, Introduction to Perturbation Techniques, John Wiley & Sons, New York, 1981.

[36] J.A. Sanders and F. Verhulst, Averaging Methods in Nonlinear Dynamical Systems, Springer, New York, 1985.

[37] S.L. Lau and Y.K. Cheung, Amplitude incremental variational principle for nonlinear vibration of elastic systems, ASME J. Appl. Mech. 48 (1981) 959–964.

[38] S.L. Lau and S.W. Yuen, Solution Diagram Of Non-Linear Dynamic Systems By The IHB Method, J. Sound Vibration 167 (1993) 303–316.

[39] A. Raghothama and S. Narayanan, Bifurcation and chaos in escape equation model by incremental harmonic balancing, Chaos, Solitons Fractals 11 (2000) 1349–1363.

[40] A. Raghothama and S. Narayanan, Bifurcation and chaos of an articulated loading platform with piecewise non-linear stiffness using the incremental harmonic balance method, Ocean Engrg. 27 (2000) 1087–1107.

[41] K.-C. Woo, A.A. Rodger, R.D. Neilson, M. Wiercigroch, Application of the harmonic balance method to ground moling machines operating in periodic regimes, Chaos, Solitons & Fractals 11(15) (2000) 2515–2525.

[42] J.H. Shen, K.C. Lin, S.H. Chen, et al, Bifurcation and route-to-chaos analyses for Mathieu-Duffing oscillator by the incremental harmonic balance method, Nonliear Dynamics 52(2008) 403–414.

[43] Y.J. Shen, S.P. Yang, X.D. Liu, Nonlinear dynamics of a spur gear pair with time-varying stiffness and backlash based on incremental harmonic balance method, International Journal of Mechanical Sciences 48(2006) 1256–1263.

[44] R. Hayes and S.P. Marques, Prediction of limit cycle oscillations under uncertainty using a Harmonic Balance method, Computers & Structures 148(2015) 1–13.

[45] G. Sun, X. Fu, Discontinuous dynamics of a class of oscillators with strongly nonlinear asymmetric damping under a periodic excitation, Communications in Nonlinear Science and Numerical Simulation 61 (2018) 230–247.

[46] L. Charroyer, O. Chiello, J.-J. Sinou, Self-excited vibrations of a non-smooth contact dynamical system with planar friction based on the shooting method, International Journal of Mechanical Sciences 144 (2018) 90–101.

[47] L. Pei, S. Wang, Dynamics and the periodic solutions of the delayed non-smooth Internet TCP-RED congestion control system via HB–AFT, Applied Mathematics and Computation 361 (2019) 689–702.

[48] W. Dai, J. Yang, B. Shi, Vibration transmission and power flow in impact oscillators with linear and nonlinear constraints International Journal of Mechanical Sciences 168 (2020) art. no. 105234.

[49] C. Pierre, A.A. Ferri and E.H. Dowell, Multi-harmonic analysis of dry friction damped systems using an incremental harmonic balance method., J. Appl. Mech. 52 (1985) 958–964.

[50] C.W., Wong, W.S., Zhang and S.L., Lau, Periodic forced vibration of unsymmetrical piecewise-linear systems by incremental harmonic-balance method, J. Sound Vib. 149(1) (1991) 91–105.

[51] S.L. Lau and W. S. Zhang, Nonlinear vibrations of piecewise-linear systems by incremental harmonic balance method, Journal of Applied Mechanics 59 (1992) 153–160.

[52] L. Xu, M. W. Lu and Q. Cao, Nonlinear vibrations of dynamical systems with a general form of piecewise-inear viscous damping by incremental harmonic balance method, Physics Letters A 301 (2002) 65–73.

[53] L. Liu, H. D. Earl and C. H. Kenneth, A novel harmonic balance analysis for the Van Der Pol oscillator, International Journal of Non-Linear Mechanics 42(1) (2007) 2-12.

[54] L. Liu and T. Kalmár-Nagy, High-dimensional Harmonic Balance Analysis for Second-order Delay-differential Equations, Journal of Vibration and Control 16 (7-8) (2010) 1189-1208.

[55] Nusse, H.E. and Yorke, J.A. *Dynamics: Numerical Explorations* (1998) Springer-Verlag, New York.

[56] R. Ju, W. Fan, W.D. Zhu, Comparison Between the Incremental Harmonic Balance Method and Alternating Frequency/Time-Domain Method, Journal of Vibration and Acoustics 143(2) (2021) 024501.